School of Natural Sciences and Mathematics

Topological Triply Degenerate Points Induced by Spin-Tensor- Momentum Couplings—Supplement

UT Dallas Author(s):

Haiping Hu
Junpeng Hou
Fan Zhang
Chuanwei Zhang

Citation:

Hu, Haiping, Junpeng Hou, Fan Zhang, and Chuanwei Zhang. 2018. "Topological Triply Degenerate Points Induced by Spin-Tensor- Momentum Couplings." Physical Review Letters 120(24): 240401:1-6, doi:10.1103/PhysRevLett.120.240401

Supplementary materials for "Topological Triply-Degenerate Points Induced by Spin-Tensor-Momentum Couplings"

Haiping Hu, Junpeng Hou, Fan Zhang, and Chuanwei Zhang*
Department of Physics, The University of Texas at Dallas, Richardson, Texas 75080, USA

Proof of $|\mathcal{C}| \leq 2$ for TDPs of Linear Hamiltonians

In this section, we unveil the geometric meaning of the topological invariant defined in Eq. (1) of the main text and give an intuitive yet rigorous proof for $|\mathcal{C}| \leq 2$ in a more general setting. To this end, we introduce a powerful tool—Majorana stellar representation [1], which maps quantum states in a high-dimensional Hilbert space onto several points (i.e., Majorana stars) on the Bloch sphere—the state space of a quantum spin-1/2 system. In this representation, any spin-1 state can be mapped to two Majorana stars on the Bloch sphere. For convenience, the integral surface $\boldsymbol{S}$ in Eq. (1) is chosen as the unit sphere.

We start with the well-known spin-1/2 system. In a chosen basis (denoted as $|\uparrow\rangle$, $|\downarrow\rangle$), an arbitrary state can be written as $|u\rangle = \cos\frac{\theta}{2}|\uparrow\rangle + e^{i\phi}\sin\frac{\theta}{2}|\downarrow\rangle$ ($0 \leq \theta \leq \pi$, $0 \leq \phi < 2\pi$). The state $|u\rangle$ is represented by a point $\boldsymbol{u} = (\sin\theta\cos\phi, \sin\theta\sin\phi, \cos\theta)$ on the Bloch sphere, with θ and ϕ denoting the colatitude and longitude in the spherical coordinate. For a Weyl point $H(\boldsymbol{k}) = -\boldsymbol{k}\cdot\boldsymbol{\sigma}$, $|u\rangle$ is the lower state at $\hat{\boldsymbol{k}} = (\sin\theta\cos\phi, \sin\theta\sin\phi, \cos\theta)$, that is, the Majorana star $\boldsymbol{u}$ on the Bloch sphere coincides with $\hat{\boldsymbol{k}}$ on the integral surface $\boldsymbol{S}$. The Chern number (monopole charge) of the Weyl point is then

$$\mathcal{C} = \frac{1}{2\pi}\oint_{\boldsymbol{S}} \boldsymbol{\Omega}(\boldsymbol{k})\cdot d\boldsymbol{S} = -\frac{1}{4\pi}\oint_{\boldsymbol{S}} d\theta d\phi\ \boldsymbol{u}\cdot\partial_\theta\boldsymbol{u}\times\partial_\phi\boldsymbol{u} = -1. \tag{S1}$$

Clearly, $\mathcal{C}$ counts how many times the Majorana star covers the Bloch sphere by varying $\hat{\boldsymbol{k}}$ on $\boldsymbol{S}$.

For a spin-1 system, any quantum state can be formulated as $|\psi\rangle = f_{-1}|1,-1\rangle + f_0|1,0\rangle + f_1|1,1\rangle$ in a given basis $|1,m\rangle$ ($m = \pm1, 0$). The basis state can be rewritten using the creation and annihilation operators $a^\dagger$, a, and $b^\dagger$, b of Schwinger bosons [2]: $|1,m\rangle = \frac{(a^\dagger)^{1+m}(b^\dagger)^{1-m}}{(1+m)!(1-m)!}|\emptyset\rangle$ ($|\emptyset\rangle$ is a vacuum state). The Schwinger bosons satisfy the standard bosonic commutation relations: $[a, a^\dagger] = [b, b^\dagger] = 1$ and all others are zero. The spin-1 operators are represented by two types of Schwinger bosons as:

$$F^+ = F_x + iF_y = a^\dagger b, \quad F^- = F_x - iF_y = b^\dagger a, \quad F_z = \frac{1}{2}(a^\dagger a - b^\dagger b), \tag{S2}$$

along with the constraint $n_a + n_b \equiv a^\dagger a + b^\dagger b = 2F$. Here n_a and n_b are the occupation numbers of Schwinger bosons. The spin-1 basis state $|1,m\rangle$ is then equivalent to the state $|n_a, n_b\rangle = |1+m, 1-m\rangle$. It is easy to verify the commutation relations for spin operators: $[F_i, F_j] = i\epsilon_{ijk}F_k$. Now the spin-1 state $|\psi\rangle$ can be factorized as [1–6]

$$|\psi\rangle = \frac{1}{N_1}\prod_{j=1}^{2}(\cos\frac{\theta_j}{2}a^\dagger + \sin\frac{\theta_j}{2}e^{i\phi_j}b^\dagger)|\emptyset\rangle, \tag{S3}$$

where N_1 is the normalization factor, and the parameters θ_j and ϕ_j can be determined by $\sum_{j=0}^{2}\frac{(-1)^j f_{1-j}}{\sqrt{(2-j)!j!}}y^{2-j} = 0$ with $y_j = \tan\frac{\theta_j}{2}e^{i\phi_j}$. By denoting $a^\dagger|\emptyset\rangle = |\uparrow\rangle$, $b^\dagger|\emptyset\rangle = |\downarrow\rangle$, it follows from Eq. (S3) that $|\psi\rangle$ is represented by the two Majorana stars located at $\boldsymbol{u}_j = (\sin\theta_j\cos\phi_j, \sin\theta_j\sin\phi_j, \cos\theta_j)$ ($j = 1, 2$) on the Bloch sphere. Within the Majorana stellar representation, now we are ready to prove $|\mathcal{C}| \leq 2$ for a spin-1 TDP.

Because the Chern number is defined on a closed two-dimensional surface $\boldsymbol{S}$ with no boundary, a nonzero Chern number indicates that we cannot choose a gauge that is continuous and single valued on the whole surface $\boldsymbol{S}$ (which yields $\mathcal{C} = 0$ by Stokes' theorem). $\boldsymbol{S}$ is then separated into different regions as sketched in Fig. S1(a). Inside each region, we can choose a smooth gauge and use the Stokes' theorem:

$$\begin{aligned} 2\pi\mathcal{C} &= \oint_{\boldsymbol{S}} \boldsymbol{\Omega}(\boldsymbol{k})\cdot d\boldsymbol{S} = \iint_{\boldsymbol{S}_a} \boldsymbol{\Omega}(\boldsymbol{k})\cdot d\boldsymbol{S} + \iint_{\boldsymbol{S}_b} \boldsymbol{\Omega}(\boldsymbol{k})\cdot d\boldsymbol{S} \\ &= \int_\Gamma \boldsymbol{A}^a\cdot d\boldsymbol{l} - \int_\Gamma \boldsymbol{A}^b\cdot d\boldsymbol{l} = \gamma^a - \gamma^b. \end{aligned} \tag{S4}$$

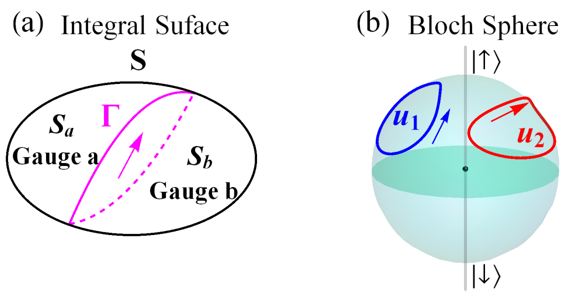

FIG. S1: (a) The integral surface $\boldsymbol{S}$ in momentum space is split into two pieces. In each piece, we can choose a smooth gauge. Γ is the boundary between the two pieces. (b) A spin-1 state is represented by two Majorana stars $\boldsymbol{u}_1$ and $\boldsymbol{u_2}$ on the Bloch sphere. The Berry phase is determined by the trajectories of two Majorana stars.

Here $\boldsymbol{A}^a$ and $\boldsymbol{A}^b$ are the gauge potentials associated with Berry curvature $\boldsymbol{\Omega}(\boldsymbol{k})$ in each region: $\boldsymbol{\nabla}\times\boldsymbol{A}^{a,b}=\boldsymbol{\Omega}(\boldsymbol{k})$. γ^a and γ^b are the accumulated Berry phases along the path Γ (i.e., the boundary of $\boldsymbol{S}_a$ and $\boldsymbol{S}_b$) under different gauges. Although $\boldsymbol{A}^{a,b}$ and $\gamma^{a,b}$ are gauge-dependent, $\boldsymbol{\Omega}(\boldsymbol{k})$ is not. From the Majorana stellar representation, the Berry phase for a spin-1 system in a chosen gauge can be elegantly formulated as [3–5]

$$\gamma=\gamma_S+\gamma_C\equiv-\sum_{j=1}^{2}\frac{1}{2}\oint(1-\cos\theta_j)d\phi_j-\frac{1}{2}\oint\frac{(d\boldsymbol{u}_1-d\boldsymbol{u}_2)\cdot(\boldsymbol{u}_1\wedge\boldsymbol{u}_2)}{3+\boldsymbol{u}_1\cdot\boldsymbol{u}_2}. \tag{S5}$$

The first term $\gamma_S=\sum_{j=1}^{2}\int_\Gamma\langle u_j|i\boldsymbol{\nabla}|u_j\rangle\cdot d\boldsymbol{l}$ describes the contributions from the solid angles subtended by the trajectories of two Majorana stars, as shown in Fig. S1(b). While the second term, which is gauge invariant [6], comes from their correlations. It is clear from Eq. (S5) that a nonzero Chern number solely comes from the gauge mismatch of the two Majorana stars. Using Stokes' theorem,

$$\begin{aligned}\mathcal{C} &= \frac{1}{2\pi}(\gamma_S^a-\gamma_S^b)=-\frac{1}{2\pi}\sum_{j=1}^{2}\mathrm{Im}[\iint_{\boldsymbol{S}_a}\langle\boldsymbol{\nabla}u_j^a|\times|\boldsymbol{\nabla}u_j^a\rangle+\iint_{\boldsymbol{S}_b}\langle\boldsymbol{\nabla}u_j^b|\times|\boldsymbol{\nabla}u_j^b\rangle]\cdot d\boldsymbol{S}\\ &= -\frac{1}{2\pi}\sum_{j=1}^{2}\mathrm{Im}\oint_{\boldsymbol{S}}(\langle\boldsymbol{\nabla}u_j|\times|\boldsymbol{\nabla}u_j\rangle)\cdot d\boldsymbol{S}=-\frac{1}{4\pi}\sum_{j=1}^{2}\oint_{\boldsymbol{S}}d\theta d\phi\ \boldsymbol{u_j}\cdot\partial_\theta\boldsymbol{u_j}\times\partial_\phi\boldsymbol{u_j}.\end{aligned} \tag{S6}$$

Geometrically, $\mathcal{C}$ is the sum of the covering numbers of the two Majorana stars on the Bloch sphere. To prove $|\mathcal{C}|\leq 2$, we only need to show, each Majorana star covers Bloch sphere at most once for our system. In another words, given two Majorana stars $\boldsymbol{u}_1$ and $\boldsymbol{u}_2$ on the Bloch sphere, we can find at most one $\hat{\boldsymbol{k}}$ on $\boldsymbol{S}$, with $\boldsymbol{u}_1$ and $\boldsymbol{u}_2$ being the projection of the lowest state of $H(\hat{\boldsymbol{k}})$ in the Majorana stellar representation.

This is done by reductio ad absurdum. We can construct a unique spin-1 state $|\psi\rangle$ (up to an irrelevant phase) using $\boldsymbol{u}_1$ and $\boldsymbol{u_2}$. Suppose both $\hat{\boldsymbol{k}}_1$ and $\hat{\boldsymbol{k}}_2$ satisfy the condition: $H(\hat{\boldsymbol{k}}_1)|\psi\rangle=e_1|\psi\rangle$ and $H(\hat{\boldsymbol{k}}_2)|\psi\rangle=e_2|\psi\rangle$, with e_1 and e_2 the lowest-state energies. Because our Hamiltonian is traceless, the sum of all the three eigenvalues must be 0. It follows that $e_{1,2}<0$ (which cannot be 0 due to the gapped spectrum on $\boldsymbol{S}$). From $\hat{\boldsymbol{k}_1}$ and $\hat{\boldsymbol{k}_2}$, we can find a point $\hat{\boldsymbol{k}}^*=\frac{e_2\hat{\boldsymbol{k}}_1-e_1\hat{\boldsymbol{k}}_2}{|e_2\hat{\boldsymbol{k}}_1-e_1\hat{\boldsymbol{k}}_2|}$ on $\boldsymbol{S}$. The linearity of Hamiltonian yields $H(\hat{\boldsymbol{k}}^*)|\psi\rangle=\frac{1}{|e_2\hat{\boldsymbol{k}_1}-e_1\hat{\boldsymbol{k}_2}|}[e_2H(\hat{\boldsymbol{k}}_1)|\psi\rangle-e_1H(\hat{\boldsymbol{k}}_2)|\psi\rangle]=0$, in contradiction to the traceless nature of the Hamiltonian. Therefore, there is at most one $\hat{\boldsymbol{k}}$ on $\boldsymbol{S}$ for any two given Majorana stars $\boldsymbol{u}_1$ and $\boldsymbol{u}_2$ on the Bloch sphere. This concludes that $|\mathcal{C}|\leq 2$ in Eq. (S6).

For a linear Hamiltonian with $H(\mathbf{k})=-H(-\mathbf{k})$, we have $C_{+1}=-C_{-1}$ for the upper and lower bands and $C_0=0$ for the middle band. $|\mathcal{C}_n|\leq 2$ determines that there are only three types of TDPs, classified by $\mathcal{C}=\pm2,\pm1,0$, as discussed in the main text. We note that in the above proof, only the $\boldsymbol{k}$-linear and traceless properties of the Hamiltonians are used. Therefore, our classification of TDPs is quite general and can be used for all spin-vector and spin-tensor momentum coupling cases, given the fact that all the spin-vectors and spin-tensors are traceless. Finally, although we consider the traceless Hamiltonians in the above proof, any additional spin-independent linear term such as ηk_z in the Hamiltonian only rotates the eigenspectrum in the momentum space without changing the eigenstates, and therefore all topological invariances and topological phase transitions do not change.

An extended model for TDPs

Besides the simple model with one spin-tensor momentum coupling term in the main text, the above general classification of TDPs also applies to more complicated models with two spin-tensors coupled to momenta, that is,

$$H(\mathbf{k}) = \mathbf{k}\cdot\mathbf{F} + \gamma_1 k_y N_{ij} + \gamma_2 k_z N_{i'j'}. \tag{S7}$$

The first term is the standard spin-vector-momentum coupling. Without loss of generality, the two spin-tensors N_{ij} and $N_{i'j'}$ are respectively coupled to k_y and k_z. γ_1 and γ_2 are the coupling strengths. In Table I, we have listed all the possible new types of TDPs.

N_{ij} \ $N_{i'j'}$	N_{xx}	N_{xy}	N_{yy}	N_{xz}	N_{yz}	N_{zz}
N_{xx}	×	×	×	III	III	II
N_{xy}	III	III	III	III	III	II,III
N_{yy}	II	II	II	II,III	II,III	II,III
N_{xz}	×	×	×	III	III	II
N_{yz}	III	III	III	III	II,III	II,III
N_{zz}	×	×	×	III	III	II

TABLE I: Type-II and type-III TDPs induced by two spin-tensor-momentum coupling terms via tuning their strengths γ_1 and γ_2. "×" means the corresponding spin-tensor-momentum couplings cannot change the type of the original TDP at $\gamma_1 = \gamma_2 = 0$, which is always type-I.

It is clear from Table I that all induced TDPs still belong to the three types, classified by different Chern numbers: $\mathcal{C} = \pm 2, \pm 1, 0$. The inclusion of more spin-tensor-momentum couplings can trigger more topological phase transitions, due to the level crossings induced by these terms. Similarly, we can discuss these level crossings, Zeeman splittings, etc. Moreover, we have checked all $6\times 6\times 6 = 216$ cases with three spin-tensors coupled into the Hamiltonian. These results are in consistent with our classification and general discussions.

Calculation of the topological invariant $\mathcal{C}$

For a given Hamiltonian $H(\boldsymbol{k})$, we can calculate its three eigenstates $|\psi_n(\boldsymbol{k})\rangle$, from which we can determine the Berry curvature $\mathbf{\Omega}_n(\mathbf{k})$. The Chern number of each band is defined as $\mathcal{C}_n = \frac{1}{2\pi}\oint_{\boldsymbol{S}} \mathbf{\Omega}_n(\mathbf{k})\cdot d\mathbf{S}$, where the integral surface $\mathbf{S}$ is chosen as a sphere of radius k around the TDP, and the surface element $d\mathbf{S} = k^2 \sin\theta d\theta d\phi \frac{\mathbf{k}}{k}$.

For the standard Hamiltonian $\boldsymbol{k}\cdot\boldsymbol{F}$, the eigenvalues are $-k, 0, k$; by taking $\boldsymbol{k} = k(\sin\theta\cos\phi, \sin\theta\sin\phi, \cos\theta)$, the corresponding eigenstates are $|-1\rangle = \left(\sin^2\frac{\theta}{2}e^{-i\phi}, -\frac{\sin\theta}{\sqrt{2}}, \cos^2\frac{\theta}{2}e^{i\phi}\right)^T$, $|0\rangle = \left(-\frac{\sin\theta}{\sqrt{2}}e^{-i\phi}, \cos\theta, \frac{\sin\theta}{\sqrt{2}}e^{i\phi}\right)^T$, $|1\rangle = \left(\cos^2\frac{\theta}{2}e^{-i\phi}, \frac{\sin\theta}{\sqrt{2}}, \sin^2\frac{\theta}{2}e^{i\phi}\right)^T$. The resulting Berry curvature for each band is found to be $\mathbf{\Omega}_n(\mathbf{k}) = -n\mathbf{k}/k^3$, yielding $\mathcal{C}_n = \frac{1}{2\pi}\int_0^\pi k^2\sin\theta d\theta \int_0^{2\pi} d\phi(-n\frac{k}{k^3}) = -n\int_0^\pi \sin\theta d\theta = -2n$. For comparison, the Berry curvature of a spin-1/2 is $\mathbf{\Omega}_n(\mathbf{k}) = -n\frac{\mathbf{k}}{2k^3}$ [7], which gives $\mathcal{C}_n = -n$. As $n = \mp 1$, $\mathcal{C}_n = \pm 1$.

For a general Hamiltonian with spin-tensors, the eigenstates and Berry curvatures cannot be determined analytically, therefore all calculations are done numerically.

Determination of phase transition points

The inclusion of spin-tensors N_{ij} can induce a series of topological phase transitions, accompanied by level-crossings in $\boldsymbol{k}$ space. To determine these phase transition points and level-crossing lines analytically, we utilize the traceless property of the Hamiltonian (all the spin-vectors F_i and spin-tensors N_{ij} are traceless), which dictates that the sum of the three eigenvalues is zero. For our model (2) with $\alpha \neq 0$, $H(\boldsymbol{k}) = k_x F_x + k_y F_y + \alpha k_z (F_z + \gamma N_{ij})$, here $\gamma = \beta/\alpha$. The topological properties would not change by rescaling k_z. For simplicity, we directly set $\alpha = 1$ and the integral surface $\boldsymbol{S}$ is chosen as the unit sphere with $k = 1$. Suppose two bands touch at some specific $\boldsymbol{k}$, at which the three eigenenergies are given by E_a, E_a, and $-2E_a$, then

$$\det(xI - H(\boldsymbol{k})) = (x - E_a)(x - E_a)(x + 2E_a) = x^3 - 3E_a^2 x + 2E_a^3 \equiv x^3 + d_1 x + d_0, \tag{S8}$$

where d_1 and d_0 satisfy $P(\boldsymbol{k}) \equiv -d_1^3/27 - d_0^2/4 = 0$. In the following, we determine the phase transition conditions using $P(\mathbf{k})$. If $P(\mathbf{k})$ cannot be zero, then there is no phase transitions as no level crossings are allowed by tuning parameters. For the 6 spin-tensors, we find the following results (by setting $y = k_z^2\gamma^2$).

(A) N_{xx}, N_{yy}, and N_{xy} would not induce any band crossing. Consider N_{xx} as an example. $P(\boldsymbol{k}) = k_x^2 y^2/27 + (-k_x^4/4 + k_x^2/6 + 1/108)y + 1/27$. As $k = 1$, $P(\mathbf{k}) \geq k_x^2 y^2/27 + (-k_x^2/4 + k_x^2/6 + k_x^2/108)y + 1/27 = k_x^2(y-1)^2/27$. Here "=" is exact for $|k_x| = 1$, hence $y \neq 1$ on the unit sphere $\boldsymbol{S}$ and we have $P(\mathbf{k}) > 0$. Similarly, we have

$$N_{yy}: \ P(\boldsymbol{k}) = k_y^2 y^2/27 + (-k_y^4/4 + k_y^2/6 + 1/108)y + 1/27 \geq k_y^2(y-1)^2/27 > 0;$$
$$N_{xy}: \ P(\boldsymbol{k}) = y^3/1728 + y^2/144 - k_x^2 k_y^2 y/4 + y/36 + 1/27 \geq y^3/1728 + y^2/144 - 5y/144 + 1/27 > 0.$$

For all the above three cases, the TDP is still type-I.

(B) For N_{zz}, $P(\boldsymbol{k}) = k_z^2 y^2/27 + (-k_z^4/4 + k_z^2/6 + 1/108)y + 1/27 \geq k_z^2(y-1)^2/27 \geq 0$. "=" is valid only when $k_z^2 = 1$ and $\gamma^2 = 1$, which is the level-crossing point. Specifically, for $\gamma = 1$, the lower (upper) band and middle band touch at $k_z = 1(-1)$; for $\gamma = -1$, the upper (lower) band and middle band touch at $k_z = 1(-1)$.

(C) For N_{xz}, $P(\boldsymbol{k}) = y^3/1728 + y^2/144 - k_x^2 k_z^2 y/4 + y/36 + 1/27 \geq y^3/1728 + y^2/144 - 5y/144 + 1/27 \geq 0$. "=" is valid when $\gamma = \pm 2$ and $k_x^2 = k_z^2 = 1/2$. At $\gamma = 2$, the lower band and middle band touch at $\pm k_z = k_x = 1/\sqrt{2}$. The upper band and middle band touch at $\pm k_z = -k_x = 1/\sqrt{2}$. Similar analysis can be applied to another transition point $\gamma = -2$. Note that for N_{yz} the results would be the same, by considering $k_y \to k_x$ and $F_y \to F_x$.

(D) $\alpha = 0$. In this case, $H(\boldsymbol{k}) = k_x F_x + k_y F_y + \beta k_z N_{ij}$. For N_{xx}, N_{xy}, N_{yy}, and N_{zz}, there exist nodal lines where two bands touch in the band structure (the triply-degenerate node is not the only degenerate point). Thus the Chern number is ill-defined. For N_{xz} and N_{yz}, the eigenenergies of $H(\boldsymbol{k})$ are given by 0, and $\pm\sqrt{k_x^2 + k_y^2 + k_z^2\beta^2/4}$. The band structure is adiabatically connected to the case (C) with $|\gamma| > 2$.

As a final remark, the function $P(\boldsymbol{k})$ can also be used to determine the splitting of TDPs.

Splitting of TDPs by a Zeeman term

A small Zeeman term εF_z breaks the triple degeneracy at $\boldsymbol{k} = 0$ for type-I and type-II TDPs described by the Hamiltonian (2). As a result, TDPs break into three doubly degenerate Weyl points located at $W_\pm = (0, 0, -\varepsilon/(\alpha \pm \beta))$ and $W_3 = (0, 0, -\varepsilon/\alpha)$. Near these three nodes with $|\delta\mathbf{k}| \ll 1$, the Hamiltonian reduces to

$$H_{W_+}(\delta\mathbf{k}) = \begin{pmatrix} (\alpha+\beta)\delta k_z & (\delta k_x - i\delta k_y)/\sqrt{2} & 0 \\ (\delta k_x + i\delta k_y)/\sqrt{2} & 0 & (\delta k_x - i\delta k_y)/\sqrt{2} \\ 0 & (\delta k_x + i\delta k_y)/\sqrt{2} & \frac{2\alpha\varepsilon}{\alpha+\beta} \end{pmatrix}, \tag{S9}$$

$$H_{W_-}(\delta\mathbf{k}) = \begin{pmatrix} -\frac{2\beta\varepsilon}{\alpha-\beta} & (\delta k_x - i\delta k_y)/\sqrt{2} & 0 \\ (\delta k_x + i\delta k_y)/\sqrt{2} & 0 & (\delta k_x - i\delta k_y)/\sqrt{2} \\ 0 & (\delta k_x + i\delta k_y)/\sqrt{2} & (-\alpha+\beta)\delta k_z \end{pmatrix}, \tag{S10}$$

$$H_{W_3}(\delta\mathbf{k}) = \begin{pmatrix} -\frac{\beta\varepsilon}{\alpha} + (\alpha+\beta)\delta k_z & (\delta k_x - i\delta k_y)/\sqrt{2} & 0 \\ (\delta k_x + i\delta k_y)/\sqrt{2} & 0 & (\delta k_x - i\delta k_y)/\sqrt{2} \\ 0 & (\delta k_x + i\delta k_y)/\sqrt{2} & -\frac{\beta\varepsilon}{\alpha} + (-\alpha+\beta)\delta k_z \end{pmatrix}. \tag{S11}$$

Therefore the effective two-band Hamiltonians can be expressed as

$$H_{W_+}(\delta\boldsymbol{k}) = \frac{1}{\sqrt{2}}\delta k_x \sigma_x + \frac{1}{\sqrt{2}}\delta k_y \sigma_y + \frac{\alpha+\beta}{2}\delta k_z \sigma_z + \frac{\alpha+\beta}{2}\delta k_z I_2 + O(\delta k^2), \tag{S12}$$

$$H_{W_-}(\delta\boldsymbol{k}) = \frac{1}{\sqrt{2}}\delta k_x \sigma_x + \frac{1}{\sqrt{2}}\delta k_y \sigma_y + \frac{\alpha-\beta}{2}\delta k_z \sigma_z + \frac{\beta-\alpha}{2}\delta k_z I_2 + O(\delta k^2), \tag{S13}$$

up to the linear order of $\delta\boldsymbol{k}$ and

$$H_{W_3}(\delta\boldsymbol{k}) = \alpha\delta k_z \sigma_z - \frac{\alpha}{2\beta\varepsilon}[(\delta k_x^2 - \delta k_y^2)\sigma_x + 2\delta k_x \delta k_y \sigma_y] + (\beta\delta k_z - \frac{\beta\varepsilon}{\alpha})I_2 + O(\delta k^3), \tag{S14}$$

up to second order of $\delta\boldsymbol{k}$. The first two are Weyl points with linear dispersions along all three directions, whereas the third one is a multi-Weyl point which has a linear dispersion in the k_z direction but quadratic dispersion along the other two directions. The Chern numbers for this multi-Weyl point is $\mathcal{C}=2$. The quadratic dispersion originates from the non-direct (second-order) couplings in F_x and F_y between the degenerate energy levels ($|+1\rangle$ and $|-1\rangle$). For $|\beta|<|\alpha|$, the linear Weyl points $W_\pm$ have the same charge $\mathcal{C}=1$ ($\alpha>0$), i.e., the case for type-I TDPs. For $|\beta|>|\alpha|$, the linear Weyl points $W_\pm$ have opposite charges $\mathcal{C}=\pm1$, i.e., the case for type-II TDPs.

In the lattice model described by Eq. (3), two TDPs appear at $(0,0,\pm\arccos(-\gamma))$. By adding a Zeeman term εF_z, the TDP at $(0,0,\arccos(-\gamma))$ is split into three nodes at $k_1=\arccos[-\frac{\varepsilon}{t_0(1+\beta)}-\gamma]$, $k_2=\arccos[-\frac{\varepsilon}{t_0(1-\beta)}-\gamma]$, and $k_3=\arccos(-\frac{\varepsilon}{t_0}-\gamma)$ along the $k_x=k_y=0$ line. Around the first two degenerate nodes, the effective two-band Hamiltonians can be written as

$$H_{k_{1,2}}=\frac{1}{\sqrt{2}}(\delta k_x\sigma_x+\delta k_y\sigma_y)-\frac{t_0\sin k_{1,2}}{2}(1\pm\beta)\delta k_z\sigma_z+O(\delta k^2), \tag{S15}$$

which describe two linear Weyl points. For $\gamma=-0.5$, both Weyl points have $\mathcal{C}=-1$ for $0<\beta<1$ (type-I) and $\mathcal{C}=\pm1$ for $\beta>1$ (type-II), which are consistent with our numerical results. The third multi-Weyl point has $\mathcal{C}=-2$ and can be described by $H_{k_3}=-t_0\sin k_3\delta k_z\sigma_z+O(\delta k^2)$, whose energy dispersion is linear in the k_z direction and quadratic in the other two directions. A similar analysis can be applied to the other TDP.

Under the same perturbation, a type-III TDP is broken into four linear Weyl points located at $(k_x,k_z)=(\pm\beta\varepsilon/(\beta-2\alpha),2\varepsilon/(\beta-2\alpha)),(\pm\beta\varepsilon/(\beta+2\alpha),-2\varepsilon/(\beta+2\alpha))$ in the $k_y=0$ plane. By neglecting those constant terms, the effective two-band Hamiltonians around these Weyl points are given by

$$\begin{aligned}
H_1(\delta\boldsymbol{k}) &= \frac{1}{\sqrt{3}}(\delta k_x-\frac{\beta}{2}\delta k_z)\sigma_x+\frac{1}{\sqrt{3}}\delta k_y\sigma_y-[\frac{1}{3}\delta k_x+(\frac{\beta}{6}-\frac{2\alpha}{3})\delta k_z]\sigma_z+O(\delta k^2), && \text{(S16)}\\
H_2(\delta\boldsymbol{k}) &= \frac{1}{\sqrt{3}}(-\delta k_x-\frac{\beta}{2}\delta k_z)\sigma_x-\frac{1}{\sqrt{3}}\delta k_y\sigma_y+[\frac{1}{3}\delta k_x-(\frac{\beta}{6}-\frac{2\alpha}{3})\delta k_z]\sigma_z+O(\delta k^2), && \text{(S17)}\\
H_3(\delta\boldsymbol{k}) &= \frac{1}{\sqrt{3}}(\delta k_x+\frac{\beta}{2}\delta k_z)\sigma_x+\frac{1}{\sqrt{3}}\delta k_y\sigma_y-[\frac{1}{3}\delta k_x-(\frac{\beta}{6}+\frac{2\alpha}{3})\delta k_z]\sigma_z+O(\delta k^2), && \text{(S18)}\\
H_4(\delta\boldsymbol{k}) &= \frac{1}{\sqrt{3}}(\delta k_x-\frac{\beta}{2}\delta k_z)\sigma_x-\frac{1}{\sqrt{3}}\delta k_y\sigma_y-[\frac{1}{3}\delta k_x+(\frac{\beta}{6}+\frac{2\alpha}{3})\delta k_z]\sigma_z+O(\delta k^2). && \text{(S19)}
\end{aligned}$$

These four nodal points can be regarded as deformed Weyl points rotated by a spin-tensor N_{xz} in the $k_y=0$ plane.

Although not in the standard form, the four Weyl points are still characterized by the Chern numbers defined in Eq. (1). In principle, the topological invariants can be determined numerically, as we have done. Here, we show that several symmetry arguments can be used for determining their Chern numbers relatively. As the first two Weyl points are related by $H_1(\delta k_x,\delta k_y,\delta k_z)=H_2(-\delta k_x,-\delta k_y,\delta k_z)$, they must have the same Chern number. As the last two Weyl points are related by $H_3(\delta k_x,\delta k_y,\delta k_z)=H_4(\delta k_x,-\delta k_y,-\delta k_z)$, they must have the same Chern number, too. Note that the four Weyl points always exist even at $\alpha=0$ for a finite Zeeman splitting. By tuning α to 0, they move in the $k_y=0$ plane without merging. The entire process is adiabatic because no level touching or crossing occurs.

At $\alpha=0$, as the first and third Weyl points are related by $H_1(\delta k_x,\delta k_y,\delta k_z)=H_3(\delta k_x,\delta k_y,-\delta k_z)$, and the first and fourth Weyl points are related by $H_1(\delta k_x,\delta k_y,\delta k_z)=H_4(\delta k_x,-\delta k_y,\delta k_z)$, the first two and the last two Weyl points must have opposite Chern numbers. Therefore, a type-III TDP can be split into two pairs of Weyl points with opposite charges, as verified by our numerical results.

Experimental scheme

Here we discuss how to experimentally realize spin-vector- and spin-tensor-momentum couplings, which are crucial for engineering different types of TDPs. Consider the following three Raman beams

$$\boldsymbol{E}_{R_1,R_3}=E_{R_1,R_3}e^{\mp ik_mz}[\hat{\boldsymbol{x}}\cos(2k_0y)\mp\hat{\boldsymbol{y}}\cos(2k_0x)]\,,\quad \boldsymbol{E}_{R_2}=E_{R_2}e^{ik_1z}(i\hat{\boldsymbol{x}}+\hat{\boldsymbol{y}}).$$

The $\boldsymbol{E}_{R_1}$ and $\boldsymbol{E}_{R_3}$ fields can be formed by multiple reflections of a beam in a 3D space that is initially polarized along $\hat{\boldsymbol{x}}$ and incident in the y-z plane with an incident angle determined by $k_1^2=k_m^2+4k_0^2$. The $\boldsymbol{E}_{R_2}$ beam is a traveling wave in the z direction with a wavevector k_1. A magnetic field $\boldsymbol{B}$ is applied in the x-y plane with a $\pi/4$-angle with respect to $\hat{\boldsymbol{x}}$. The Raman couplings between the hyperfine states are contributed from both $D_1(6^2S_{1/2}\to7^2P_{1/2})$ and $D_2(6^2S_{1/2}\to7^2P_{3/2})$ lines with detunings $\Delta_{1/2}$ and $\Delta_{3/2}$, respectively. The detunings are much larger than the hyperfine structure. The resulting Raman couplings can be obtained by summing over all the transitions allowed by the selection rules. For the purpose of calculations, we need to decompose the electric field as follows:

$$\begin{aligned} \boldsymbol{E}_{R_1,R_3} &= \frac{E_{R_1,R_3} e^{\mp i k_m z}}{\sqrt{2}}\{[\cos(2k_0 y) \mp \cos(2k_0 x)]\hat{\boldsymbol{B}}_{\parallel} - [\cos(2k_0 y) \pm \cos(2k_0 x)]\hat{\boldsymbol{B}}_{\perp}\}, \\ \boldsymbol{E}_{R_2} &= \frac{E_{R_2} e^{i k_1 z}}{\sqrt{2}}[(1+i)\hat{\boldsymbol{B}}_{\parallel} + (1-i)\hat{\boldsymbol{B}}_{\perp}]. \end{aligned} \tag{S20}$$

The component parallel to (perpendicular to) $\boldsymbol{B}$ is used to induce the π (σ) transition, as illustrated in Fig. S2.

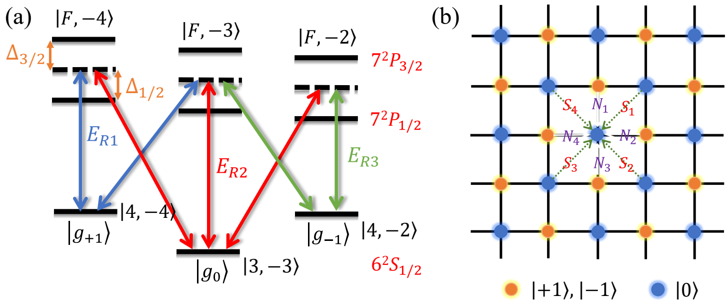

FIG. S2: (a) Optical transitions to generate Raman couplings between three hyperfine states. (b) Schematic of the tight-binding model, in which $g_{\pm 1}$ stay in one sublattice while g_0 in the other sublattice, $\boldsymbol{N}_1$ to $\boldsymbol{N}_4$ denote the nearest-neighbor bonding between different components, and $\boldsymbol{S}_1$ to $\boldsymbol{S}_4$ denote the next-nearest-neighbor bonding between the same components.

The Raman coupling between g_{+1} and g_0 comes from the following two parts by summing over all possible F:

$$\begin{aligned} M^1_{+1,0} &= \sum_{J=\frac{1}{2},\frac{3}{2}}^{F} \frac{\Omega^{J*}_{g_{+1},F,1\parallel}\Omega^{J}_{g_0,F,2-}}{\Delta_J} = \frac{\sqrt{7}E_{R_1}E_{R_2}\alpha^2_{D_1}}{12\sqrt{2}}(\frac{1}{\Delta_{3/2}} - \frac{1}{\Delta_{1/2}})(1-i)e^{i(k_1+k_m)z}[\cos(2k_0x) - \cos(2k_0y)], \\ M^2_{+1,0} &= \sum_{J=\frac{1}{2},\frac{3}{2}}^{F} \frac{\Omega^{J*}_{g_{+1},F,1+}\Omega^{J}_{g_0,F,2\parallel}}{\Delta_J} = \frac{\sqrt{7}E_{R_1}E_{R_2}\alpha^2_{D_1}}{12\sqrt{2}}(\frac{1}{\Delta_{3/2}} - \frac{1}{\Delta_{1/2}})(1+i)e^{i(k_1+k_m)z}[\cos(2k_0x) + \cos(2k_0y)]. \end{aligned}$$

Here $\Omega^J_{g_s,F,\parallel} = e\langle g_s|z|F,0,J\rangle\hat{\boldsymbol{e}}_z\cdot\boldsymbol{E}$ and $\Omega^J_{g_s,F,\pm} = e\langle g_s|e^{\pm}|F,\pm1,J\rangle\hat{\boldsymbol{e}}_{\pm}\cdot\boldsymbol{E}$ are the transition matrix elements in the basis of the circularly polarized light in the plane perpendicular to $\boldsymbol{B}$.

Similarly, the Raman coupling between g_{-1} and g_0 can be written as

$$M^1_{-1,0} = \sum_{J=\frac{1}{2},\frac{3}{2}}^{F} \frac{\Omega^{J*}_{g_{-1},F,3\parallel}\Omega^{J}_{g_0,F,2+}}{\Delta_J} = \frac{E_{R_2}E_{R_3}\alpha^2_{D_1}}{24\sqrt{2}}(\frac{1}{\Delta_{3/2}} - \frac{1}{\Delta_{1/2}})(1-i)e^{i(k_1-k_m)z}[\cos(2k_0x) + \cos(2k_0y)], \tag{S21}$$

$$M^2_{-1,0} = \sum_{J=\frac{1}{2},\frac{3}{2}}^{F} \frac{\Omega^{J*}_{g_{-1},F,3-}\Omega^{J}_{g_0,F,2\parallel}}{\Delta_J} = \frac{E_{R_2}E_{R_3}\alpha^2_{D_1}}{24\sqrt{2}}(\frac{1}{\Delta_{3/2}} - \frac{1}{\Delta_{1/2}})(1+i)e^{i(k_1-k_m)z}[\cos(2k_0x) - \cos(2k_0y)]. \tag{S22}$$

If follows that the total Raman couplings between $g_{\pm1}$ and g_0 are respectively

$$M_{+1,0} = M^1_{+1,0} + M^2_{+1,0} = M_0 e^{i(k_1+k_m)z}[\cos(2k_0x) + i\cos(2k_0y)], \tag{S23}$$

$$M_{-1,0} = M^1_{-1,0} + M^2_{-1,0} = M'_0 e^{i(k_1-k_m)z}[\cos(2k_0x) - i\cos(2k_0y)], \tag{S24}$$

where $M_0 = \frac{\sqrt{7}\alpha^2_{D_1}E_{R_1}E_{R_2}}{6\sqrt{2}\Delta_2}$, $M'_0 = \frac{\alpha^2_{D_1}E_{R_2}E_{R_3}}{12\sqrt{2}\Delta_2}$, and $\frac{1}{\Delta_2} = \frac{1}{\Delta_{3/2}} - \frac{1}{\Delta_{1/2}}$.

To remove the spatially dependent phase factor in the Raman coupling, we can use the gauge transformation $U = e^{i(k_1F_z^2 + k_mF_z)z}$, which would not affect other terms. In the rotated frame, the Raman coupling then becomes

$$H_R = \lambda k_z(k_1F_z^2 + k_mF_z) + [\cos(2k_0x) + i\cos(2k_0y)](M_0|g_{+1}\rangle\langle g_0| + M'_0|g_0\rangle\langle g_{-1}|) + \text{h.c.} \tag{S25}$$

with $\lambda = \hbar^2/m$ by neglecting those constant term. Since the spin-dependent lattice potentials have the same sign for g_{+1} and g_{-1} components, we can write the tight-binding model on a square lattice in the x-y plane as shown in

Fig. S2(b), in which $g_{\pm 1}$ stay in one sublattice while g_0 in the other sublattice. We consider the nearest-neighbor and next-nearest-neighbor hopping terms with only s-orbital of each site. The hopping between the nearest-neighbor sites are between different components induced by the Raman couplings. The hopping between the next-nearest-neighbor sites are between the same component. The effective tight-binding Hamiltonian reads

$$H_{tb} = \frac{\lambda k_z^2}{2} + H_R - \sum_{i,j}^{s=\pm1,0} t_s c_s^\dagger(\boldsymbol{r_i}) c_s(\boldsymbol{r_i} + \boldsymbol{S}_j) - \sum_{i}^{s=\pm1,0} \delta_s c_s^\dagger(\boldsymbol{r_i}) c_s(\boldsymbol{r_i}) \tag{S26}$$

$$+ \sum_{i,j} t_{so1}^{ij} c_{+1}^\dagger(\boldsymbol{r}_i) c_0(\boldsymbol{r}_i + \boldsymbol{N}_j) + \sum_{i,j} t_{so2}^{ij} c_{-1}^\dagger(\boldsymbol{r}_i) c_0(\boldsymbol{r}_i + \boldsymbol{N}_j) + \text{h.c.}, \tag{S27}$$

where the Zeeman term has been incorporated into the detunings in the ground state manifold. The coupling coefficients are

$$t_s = \int d^2\boldsymbol{r} \phi_s^{i*} \left[\frac{\lambda}{2}(k_x^2 + k_y^2) + V(\boldsymbol{r}) \right] \phi_s^j(\boldsymbol{r}), \quad t_{so1}^{ij} = \int d^2\boldsymbol{r} \phi_{+1}^{i*} M_{+1,0} \phi_0^j(\boldsymbol{r}), \quad t_{so2}^{ij} = \int d^2\boldsymbol{r} \phi_{-1}^{i*} M_{-1,0} \phi_0^j(\boldsymbol{r}). \tag{S28}$$

The spin-flipped hopping coefficients satisfy $t_{so1}^{jx,jx\pm1} = \pm t_{so1}$, $t_{so1}^{jy,jy\pm1} = \pm i t_{so1}$, $t_{so2}^{jx,jx\pm1} = \pm t_{so2}$, and $t_{so2}^{jy,jy\pm1} = \mp i t_{so2}$, as constrained by the lattice symmetry. For the spin-dependent lattice, each unit cell contains two lattice sites with primitive vectors along the two diagonal directions (lattice constant $b = \pi/k_0$). Using Fourier transformation and setting $t_{so1} = t_{so2} = \frac{t_{so}}{2\sqrt{2}}$, which can be achieved by adjusting the relative strengths of Raman beams, we obtain the following momentum-space Hamiltonian

$$H_{3D}(\boldsymbol{k}) = \frac{\lambda k_z^2}{2} - 4T_s \cos(k_x a)\cos(k_y a) - \Lambda_s + \lambda k_z (k_1 F_z^2 + k_m F_z) + t_{so} F_x \sin(k_x a) + t_{so} F_y \sin(k_y a). \tag{S29}$$

Here $a = \frac{\pi}{\sqrt{2}k_0}$, and $k_x = (k_+ + k_-)/\sqrt{2}$, $k_y = (k_+ - k_-)/\sqrt{2}$ are lattice momenta along x and y directions. $T_s = \text{diag}(t_{+1}, t_0, t_{-1})$ and $\Lambda_s = \text{diag}(\delta_{+1}, \delta_0, \delta_{-1})$ are diagonal matrices for tunneling and detuning. When $t_{+1} = t_0 = t_{-1}$ and $\delta_{+1} = \delta_0 = \delta_{-1}$, i.e., no Zeeman term, there exist two TDPs in the 2D Brillouin zone spanned by (k_x, k_y). They are located at $(0,0)$ and $(\pi, 0)$. (Note that $(0,0)$ and (π,π) ($(\pi,0)$ and $(0,\pi)$) are the same momenta by folding back to the first Brillouin zone spanned by (k_+, k_-)). By expanding the above Hamiltonian around the two points, we obtain the following low-energy Hamiltonians (setting $a = 1$)

$$H_1(\delta\boldsymbol{k}) = \lambda \delta k_z (k_1 F_z^2 + k_m F_z) + t_{so} \delta k_x F_x + t_{so} \delta k_y F_y, \tag{S30}$$

$$H_2(\delta\boldsymbol{k}) = \lambda \delta k_z (k_1 F_z^2 + k_m F_z) - t_{so} \delta k_x F_x + t_{so} \delta k_y F_y, \tag{S31}$$

which are similar to the Hamiltonian (2). The two TDPs have the opposite Chern numbers. When t_s are not equal, the resulting Zeeman field at the two points may be compensated by choosing suitable detuning δ_s. In this case, one of two TDPs will survive, whereas the other one will be broken into two Weyl points with opposite Chern numbers.

* Electronic address: chuanwei.zhang@utdallas.edu

[1] E. Majorana, *Atomi orientati in campo magnetico variabile*, Nuovo Cimento **9**, 43 (1932).

[2] J. Schwinger, Quantum Theory of Angular Momentum, edited by L. C. Biendenharn and H. Van Dam (Academic Press, New York, 1965).

[3] J. H. Hannay, *The Berry phase for spin in the Majorana representation*, J. Phys. A **31**, L53 (1998).

[4] P. Bruno, *Quantum geometric phase in Majorana stellar representation: Mapping onto a many-body Aharonov-Bohm phase*, Phys. Rev. Lett. **108**, 240402 (2012); Q. Niu, *Viewpoint: A quantum constellation*, Physics **5**, 65 (2012).

[5] H. D. Liu and L. B. Fu, *Representation of Berry phase by the trajectories of Majorana stars*, Phys. Rev. Lett. **113**, 240403 (2014).

[6] R. Barnett, D. Podolsky, and G. Refael, *Geometrical approach to hydrodynamics and low-energy excitations of spinor condensates*, Phys. Rev. B **80**, 024420 (2009).

[7] see B. Andrei Bernevig and Taylor L. Hughes's book "Topological Insulators and Topological Superconductors", Page. 11, Eq. (2.23).